



INSTITUT DE FRANCE  
Académie des sciences

# *Comptes Rendus*

---

## *Mécanique*


Muhammad Hafizh, Asan G. A. Muthalif, Jamil Renno, M. R. Paurobally, Mohamed A. Arab, Issam Bahadur and Hassen Ouakad

**A hybrid piezoelectric–electromagnetic nonlinear vibration energy harvester excited by fluid flow**

Volume 349, issue 1 (2021), p. 65-81.

<https://doi.org/10.5802/crmeca.74>

© Académie des sciences, Paris and the authors, 2021.  
*Some rights reserved.*

 This article is licensed under the  
CREATIVE COMMONS ATTRIBUTION 4.0 INTERNATIONAL LICENSE.  
<http://creativecommons.org/licenses/by/4.0/>



*Les Comptes Rendus. Mécanique* sont membres du  
Centre Mersenne pour l'édition scientifique ouverte  
[www.centre-mersenne.org](http://www.centre-mersenne.org)



---

Synthesis / Synthèse

# A hybrid piezoelectric–electromagnetic nonlinear vibration energy harvester excited by fluid flow

Muhammad Hafizh<sup>a</sup>, Asan G. A. Muthalif<sup>\*, a</sup>, Jamil Renno<sup>a</sup>,  
M. R. Paurobally<sup>a</sup>, Mohamed A. Arab<sup>a</sup>, Issam Bahadur<sup>b</sup> and Hassen Ouakad<sup>b</sup>

<sup>a</sup> Department of Mechanical and Industrial Engineering, Qatar University, Qatar

<sup>b</sup> Mechanical & Industrial Engineering, Sultan Qaboos University, Oman

*E-mails:* muhammad.hafizh@qu.edu.qa (M. Hafizh), drasan@qu.edu.qa (A. G. A. Muthalif), jamil.renno@qu.edu.qa (J. Renno), mpaurobally@qu.edu.qa (M. R. Paurobally), ma1108785@qu.edu.qa (M. A. Arab), bahdoor@squ.edu.om (I. Bahadur), houakad@squ.edu.om (H. Ouakad)

**Abstract.** Energy harvesting mechanisms can be used to extract energy from ambient surroundings to power small electronic devices, which has a significant advantage in realizing self-sustaining wireless devices. The proposed design of this study uses the internal fluid flow within a pipe and takes advantage of the fluid–structure interaction through flow-induced vibration of a bluff body. The hybrid harvester uses the vibration to convert electrical energy through a piezoelectric material and an electromagnetic oscillator that can be tuned to resonate at the oscillation frequency. A numerical solver was used to estimate harvestable voltage for this submerged hybrid energy harvester model by using ordinary differential equations. A computational study was used to optimize the performance of the bluff bodies under the influence of the vortices for circular, triangular, ellipse, and quadrilateral shapes. Wake development was seen in the circular and triangular shapes with the ellipse having the lowest turbulence kinetic energy among the shapes. Structural deflection of the beam under resonance was compared for the different shapes, which displayed better results for triangular and elliptical bluff bodies.

**Keywords.** Hydrokinetic energy harvesting, Piezoelectric harvester, Electromagnetic, Shape optimization, Internal flow of fluid in a pipe.

*Manuscript received 8th November 2020, revised 25th January 2021, accepted 26th January 2021.*

## 1. Introduction

With the growing maturity in efficient devices and energy harvesting mechanisms, the advances in self-sustaining powered devices has the potential to improve the sustainability of energy use and service life. Piezoelectric energy harvesting (PEH) has received an extensive amount

---

\* Corresponding author.

of research and development over the last decades due to its versatility in converting kinetic energy into electric power and store it in batteries or capacitors [1]. Previous work has provided useful insights into the well-optimized design of piezoelectric energy harvesting as well as the driving mechanisms behind it [2]. More recent work has shown the potential of realizing self-sustaining PEHs for wireless transmission devices with a power storage by adding an IGBT H-Bridge and bi-directional buck boost converter [3]. The addition of a tip mass (i.e., cylindrical bluff body) adds a design parameter that can tune the resonance frequency and maximize power output [4, 5]. Although PEH work in liquid media has been limited compared to that done in air, the advancements in piezoelectric materials, mechanisms, and analytical models have helped to improve the conversion of vibratory energy to electrical energy [6]. Adding a cylindrical bluff body helps increase the deflection of the piezoelectric beam due to the phenomenon of vortex-induced vibrations (VIVs), which has been studied extensively [7–10]. Gao *et al.* [11] investigated the use of a piezoelectric cantilever with a cylindrical extension through flow-induced vibration (FIV) near the natural frequency. They concluded that the generated voltage output through turbulent flow would be sufficient to power small electronics. This is because harvesting energy from fluid flow gives rise to periodic oscillations found in “von Karman’s” vortex street, where it was suggested that conversion efficiency increases with decreasing harvester size due to the oscillation frequency [12]. Furthermore, work done on upright PEHs have also provided derived theoretical expressions and experimental results that lay the groundwork for multiple array orientations and structural design [13]. Recently, more work has emerged from FIVs of other cross-sectional geometries and forced vibration modes are classified as buffeting, galloping, and fluttering [14]. Aramendia *et al.* [15] have also shown that geometric differences and optimization parameters can influence the performance of PEH such that a U-shaped performs better than a circular bluff body. Abdelkefi *et al.* [16] looked at the performance of PEHs with a square, triangular, and D-shaped bluff bodies in galloping-based vibrations in air, which highlighted the importance of electromechanical coupling on a system to extract maximum amount of harvested power. Akaydin *et al.* [17] also demonstrated the importance of the coupling of aerodynamic, electrical, and mechanical interactions that play a significant impact on the power output, damping, and electrical resistance. Sun *et al.* [18] also investigated the effects of VIVs and galloping at lower velocities of water flow through Van der Pol models and quasi-steady models, respectively. The experimental work in the paper also outlined that galloping energy harvested is more superior to VIV and that a larger lift force leads to larger oscillation amplitudes and harvested power. Experimental open channel energy harvesting with macrofiber composites submerged in water was also conducted by Sun *et al.* [19] who showed that cylindrical bluff bodies perform better at lower velocities due to VIV but do not perform as well as triangular prisms as at higher velocities due to the additional galloping effects.

Work on combined FIV energy harvesters have also emerged in the research field. Also, the addition of an electromagnetic oscillator placed outside of the beam working in conjunction with a piezoelectric harvester beam has the potential to further increase the power output of the system by up to 30% [20]. The application of piezoelectric harvesters can be extended to be modeled with sea waves using wave models [21]. Also, a combined hybrid system was proposed by Zhao *et al.*, where the oscillations of FIV could harvest energy through piezoelectric strain and electromagnetic induction [22]. Zang *et al.* [23] also demonstrated that the use of magnetic forces on broadband energy harvesting through VIV can increase the level of harvester power by 29% and increase the synchronization region by 138%.

In this paper, we present a compact form factor hybrid energy harvester that can collect power from a fluid stream through a piezoelectric material and electromagnetic oscillator. The long-term goal would be to use the harvester in a system as part of a self-sustaining diagnostic and data collection system. The process of energy harvesting is especially useful in areas where access to a

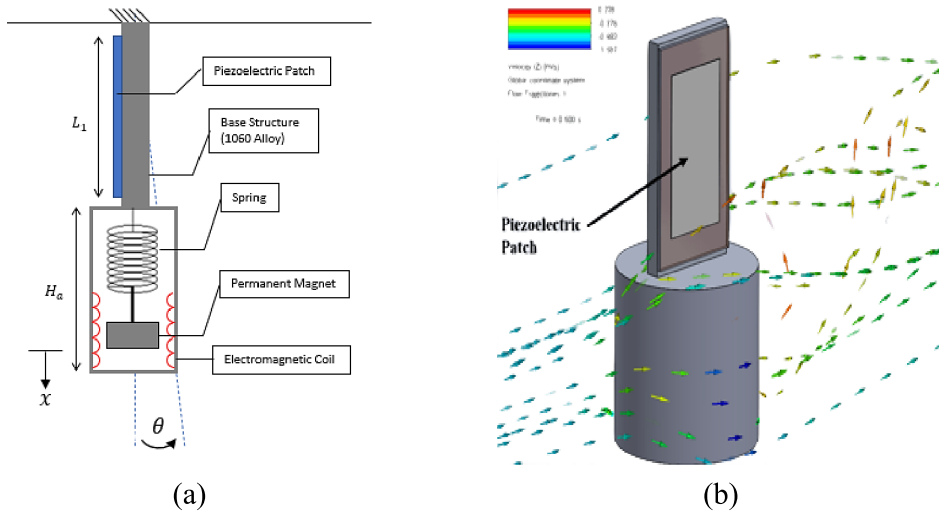


**Figure 1.** Electromagnetically coupled piezoelectric energy harvesting system: (a) Schematic and components; (b) Direction of water flow during harvesting.

surplus power input is not readily available and can instead be collected from renewable ambient sources and utilized for process monitoring purposes.

This paper is organized as follows. Section 2 presents the mathematical model of the proposed energy harvester. The computational setup of the wake generation and flow simulations are presented in Section 3. Numerical results of the mathematical model are seen in Section 4. The optimization study for different bluff bodies is presented in Section 5 and conclusions to this study are summarized in Section 6.

## 2. Mathematical model of a piezoelectric energy harvester coupled with an electromagnetic oscillator

The main goal of the current work is to increase the energy harvested from a hybrid energy harvester from FIV as shown in Figure 1. The harvester comprises of a piezoelectric patch that is mounted on a cantilevered beam with electromagnetic oscillator inside a bluff body at its free tip. The generation of “von Karman” vortex shedding around a cylindrical bluff body creates the transverse vibrations normal to the direction of the flow of water. The parameters used for the system are defined in Table 1 and additional nomenclature in Table 2. The material for the beam and oscillator used in this study is 1060 aluminum alloy since it provides good elastic properties to induce internal strain on the piezoelectric patch. The piezoelectric patch selected was polypropylene for having a high fatigue resistance to aqueous solutions [24] and inert for drinking water applications [25].

### 2.1. Piezoelectric system

The harvester model is made up of a vertical piezoelectric beam with an attached tip mass that oscillates because of the water flow through the pipe with speed defined as  $V_{\text{water}}$  and the corresponding force,  $F_L$  induced by the water on the cylinder. The turbulence caused by the bluff body results in oscillations acting perpendicular to the flow of water. The FIV outputs the voltage for the piezoelectric element defined as  $V(t)$ . The proposed hydro-electromechanical

**Table 1.** Modeled parameters

Symbol	Description	Value	Units
$\rho_{\text{piezo}}$	Piezoelectric material density	5319	kg/m <sup>3</sup>
$\rho_{\text{cylinder}}$	Circular cylinder oscillator density	2700	kg/m <sup>3</sup>
$\rho_{\text{fluid}}$	Fluid density	999.06	kg/m <sup>3</sup>
$D$	Cylinder bluff-body diameter	0.04512	m
$L_1$	Length of layer	0.038	m
$L$	Length of the beam	0.13	m
$b$	Width of the beam	0.05	m
$h$	Thickness of the beam	0.006	m
$H_a$	Cylinder height	0.06	m
$J_{wt}$	Cylinder inertia moment	$4.069 \times 10^{-7}$	kg·m <sup>2</sup>
$C_L$	Lift coefficient evolution	1	–

model outlines the equation of motion for the harvester subjected to the incoming water flow submerged in a pipe and affects the lift coefficient,  $C_L$  evolution at the studied water speed as expressed in (1)–(6) for 1.24 m/s [26]:

$$a_2\ddot{\theta} + a_3\dot{\theta} + a_4\theta = a_1 T_{\text{Hydro}} \quad (1)$$

$$a_1 = \frac{C_L \cdot \rho_{\text{fluid}} \cdot D \cdot V_{\text{water}}^2 \cdot H_a \cdot (2L - H_a)}{4} \approx 0.03202 \quad (2)$$

$$a_2 = J_{wt} + L_1 \rho_{\text{piezo}} A a^2 \approx 2.919 \times 10^{-3} \quad (3)$$

$$a_3 = f + \frac{\alpha^2 \cdot a^2}{K_p \cdot K_{\text{trans}}} \approx 4.612 \times 10^{-3} \quad (4)$$

$$a_4 = \frac{K \cdot a^2}{K_{\text{trans}}} \approx 0.01579 \quad (5)$$

$$T_{\text{hydro}} \approx \sin \omega t. \quad (6)$$

Here  $\theta$  refers to the angular displacement of the deformed beam as shown in Figure 1 resulting in a transverse motion of the bluff body oscillating perpendicular to the direction of water flow. The input hydro-mechanical torque  $T_{\text{hydro}}$  modeled after the water flow represents a sinusoidal waveform and evolution of lift coefficient is modeled as a constant. Thus, the voltage output generated across the piezoelectric patch (with a load  $R_L$  and having an electromechanical coupling coefficient  $\Theta$ ) with an added tip mass can be expressed as the following in (7) [27]:

$$\frac{V_{\text{piezoelectric}}(t)}{R_L} + C^s \dot{V}_{\text{piezoelectric}}(t) - \Theta L \dot{\theta}(t) = 0. \quad (7)$$

## 2.2. Coupled electromagnetic system

Adding another harvesting mechanism to the existing structure is an added contribution in implementing a hybrid energy harvester for hydrokinetic applications. It involves a spring attached to a permanent magnet mass within a coil of wire (Figure 1(a)), the movement of the harvesting structure causes springs oscillations. Soti *et al.* [28] summarized that the maximum average power does not significantly change for variations in coil length and coil radius. According to Faraday's law of electromagnetic induction, an electromotive force (emf) is produced by the movement of a magnet within a coil of wire because of a change in the magnetic flux. Also, the emf generated is directly proportional to the change in the flux, resulting in greater energy conversion

**Table 2.** Nomenclature of hybrid energy harvester

Symbol	Description	Units
$\rho_{\text{piezo}}$	Piezoelectric material density	kg/m <sup>3</sup>
$\rho_{\text{cylinder}}$	Circular cylinder oscillator density	kg/m <sup>3</sup>
$\rho_{\text{fluid}}$	Fluid density	kg/m <sup>3</sup>
$A$	Cross section of piezoelectric	m <sup>2</sup>
$K$	Piezoelectric stiffness	N/m
$D$	Cylinder bluff-body diameter	m
$K_{\text{trans}}$	Transduction gain	–
$K_p$	Proportional gain	–
$C$	Piezoelectric capacitance	nF
$f$	Frictional coefficient	(N·m·s)/rad
$L_1$	Length of layer	m
$L$	Length of the beam	m
$b$	Width of the beam	m
$h$	Thickness of the beam	m
$H_a$	Cylinder height	m
$a$	Force application distance point	m
$\alpha$	Voltage-induced bending factor	A·s/m
$J_{wt}$	Cylinder inertia moment	kg·m <sup>2</sup>
$C^S$	Clamp capacitance for piezoelectric transducer	F
$R_L$	Load resistance	$\Omega$
$C_L$	Lift coefficient evolution	–
$\Theta$	Electromechanical coupling coefficient	N·V <sup>-1</sup>

because of the restoring oscillatory motions. Thus, the governing equation for induced emf of a disk-shaped magnet moving with a velocity  $v$  in a magnetic field  $B$  of a coil is expressed as (10):

$$\varepsilon = \oint (\vec{v} \times \vec{B}) \cdot d\vec{l}. \tag{8}$$

Once the electromagnetic coil is connected to resistive load  $R_L$ , the induced current ( $i = \varepsilon/R_L$ ) in the circuit opposes the motion of the magnet experiencing an opposing electromagnetic force because of the now present electromagnetic coupling. This reaction force acting on the magnet can be expressed in (9) [29]:

$$F = \int i d\vec{l} \times \vec{B} \cdot \hat{z}. \tag{9}$$

Equation (10) shows the expression for a single dipole magnetic moment  $\mu$ , the approximated electromagnetic force for a coil with  $N$  number of turns and vertical height  $L_{\text{coil}}$  is the coil length looped around the oscillator enclosure [29]:

$$F = \frac{\left(\frac{N}{L_{\text{coil}}} 2\pi a^2 \mu\right) v}{R_{\text{coil}}} \left[ \frac{1}{[a^2 + h]^{\frac{3}{2}}} - \frac{1}{[a^2 + (h + L)^2]^{\frac{3}{2}}} \right]^2. \tag{10}$$

If  $a$  is the internal radius of the electromagnetic coil,  $h$  is the distance from the center of the magnet to the height of the coil. The internal electrical resistance of the conduction coil  $R_{\text{coil}} = (4N(2\pi a)/\sigma\pi D^2)$  with a wire conductivity  $\sigma$ . The added benefit of having the oscillator system mounted internally is to have the freedom to retrofit the hybrid energy harvester and placed in a tandem or combined arrangement with multiple other devices like it. By shifting the resonance point of the oscillator near to the bluff-body structure, the behavior can be adjusted for a fixed water flow to maximize the harvestable energy output or to target a wider range of

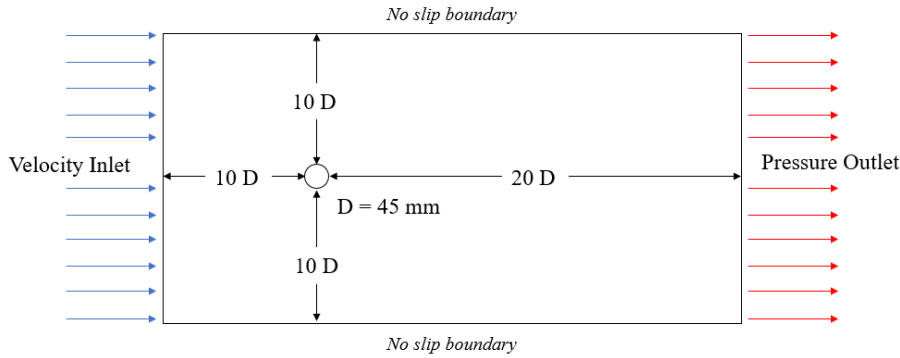


**Figure 2.** Computational domain setup and parameters.

frequencies for a broadband energy harvesting application. Since the oscillator is fixed inside the bluff body, there will be another degree of freedom for the coupled electromagnetic system that generates electricity through the vibration of the magnet. The equation of motion for such a system can be simply expressed by (11):

$$\ddot{x} + \frac{k}{m}x - (L + x)\dot{\theta}^2 - g \cos\theta + BIL_{\text{coil}} = 0. \quad (11)$$

Since the angular motion of the mass–spring system is restricted, the oscillation of the mass occurs in the vertical direction within the confined space of the bluff body. Alternatively, the use of two springs attached on each end of the magnetic mass ( $k = k_1 + k_2$ ) can also enhance the amount of power harvested by forcing the magnet to oscillate close to the center of the coil where the magnetic flux is the densest. Alternatively, springs can be replaced by two magnets of opposite polarity to the center magnet and exhibit the characteristics of a spring with a total stiffness of  $k$ . From (8),  $x$  refers to the linear displacement of the mass from the static position on the spring,  $\theta$  is angular displacement experienced by the beam expressed in (1),  $B$  is the flux density, and  $I$  is current within. Therefore, the voltage output from the electromagnetic oscillator can then be modeled as a function of the electromagnetic induction (9) and self-inductance  $L_{\text{ind}}$  as shown in (12):

$$V_{\text{electromagnetic}} = BL_{\text{coil}}\dot{x} - L_{\text{ind}}\dot{I}. \quad (12)$$

Thus, the entire harvester dynamics are expressed in (1), (7), (11), and (12).

### 3. Computational setup

The computational fluid dynamics (CFD) setup in modeling the energy harvester inside of a pipe carrying water used a two-dimensional approach to visualize the effects of the vortex shedding and wake generation across the different bluff bodies. The computational domain was made up of a velocity inlet of water (temperature: 288.15 K) of varying velocities with a width of  $20D$  nonslip boundary walls—where  $D$  is the diameter of the circular bluff body—from the center of the circular bluff body and  $10D$  upstream. The downstream length of the domain was modeled  $30D$  for wake generation and to visualize the vortex shedding over a period of 20 s. The computational domain and mesh distribution around the cylindrical bluff body is shown in Figure 2.

ANSYS Fluent v. 2020 R2 [30] solver was used in setting up the CFD simulation, Figure 3, with approximately 93,000 elements of triangular mesh with 15 inflated layers around the bluff body. The unsteady state flow was solved using unsteady Reynolds-averaged Navier Stokes

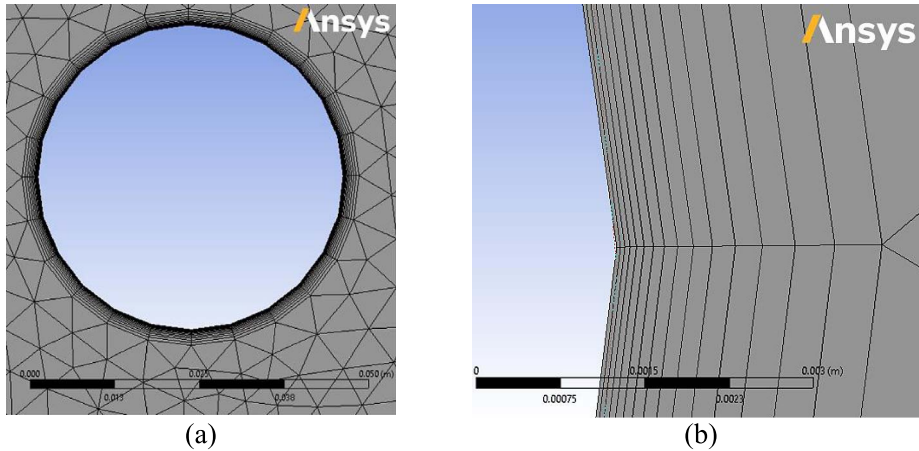


**Figure 3.** Mesh generation: (a) view of mesh around circular body with triangular generation; (b) close-up of inflated mesh around body.

**Table 3.** Mesh independence study

$Re$	Mesh definition			Richardson extrapolation		
	Coarse	Medium	Fine	$Re$	$p$	$R$
12,000	0.94	1.02	1.18	1.23	0.98	1.97

**Table 4.** Comparison between simulation and experimental results at  $Re = 12,000$

Measurement	Simulation	Experiments
$C_{D,mean}$	1.19	1.10–1.20 [33]
$C_{L,RMS}$	0.498	0.435 [34]

(URANS) equations. Since the Reynold’s number ( $Re = \rho vD/\mu$ ) exceeds the transition interval, a turbulent transport model  $k-\omega$  SST viscous model developed by Menter [31] was used. The time interval of 0.002 s and 15 iteration per time step was selected because it provided adequate values to see the vortex shedding and convergence. A semi-implicit method for pressure-linked equations (SIMPLE) algorithm-based solver was used which balances out computational expense and convergence rates. Second-order upwind spatial discretization and second-order implicit transient formulation settings were also applied to this simulation. The mesh was refined to keep  $y^+$  around the body below 1. A mesh independence study has been performed to verify the selected mesh resolution by using the Richardson extrapolation method [32] summarized in Table 3 by comparing the CFD results of drag coefficient for three different meshes of varying elements: 23,500 (coarse), 47,000 (medium), 94,000 (fine). The results of the fine mesh predict the drag coefficients adequately and was used for subsequent simulations. A good agreement between the numerical solution and experiments from literature are summarized in Table 4 by comparing the lift ( $C_L$ ) and drag ( $C_D$ ) coefficients [33, 34].

#### 4. Results

To visualize the response of the harvester, MATLAB was used to solve the coupled differential equations (1), (7), (11), and (12). For this set of nonlinear differential equations, an ordinary



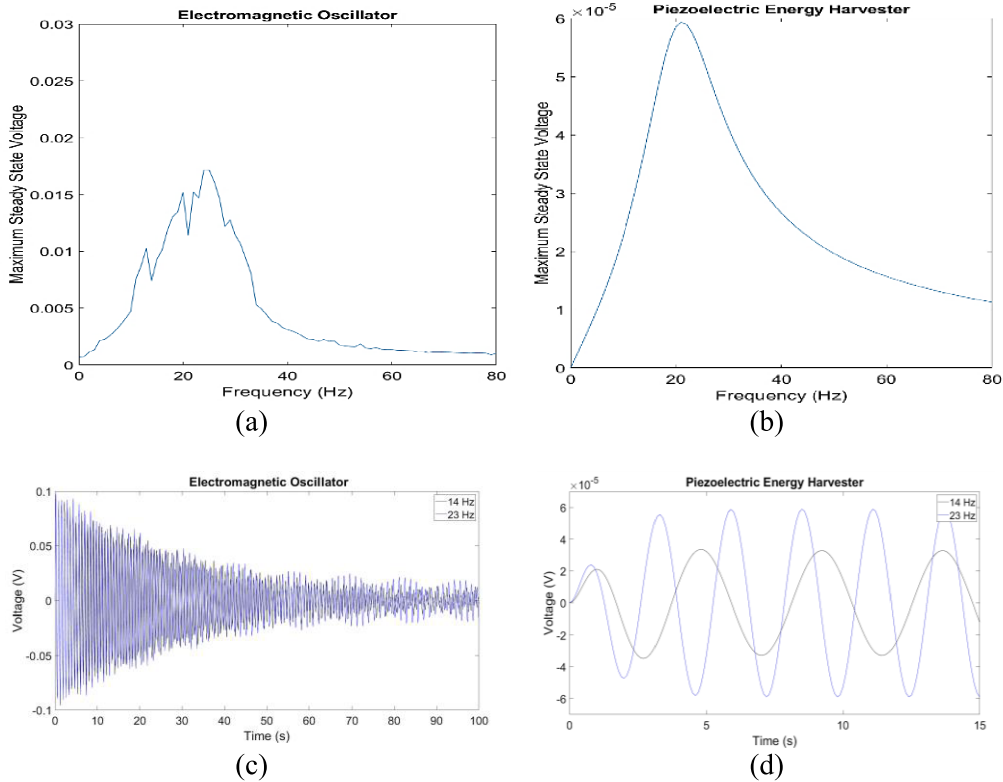


**Figure 4.** MATLAB simulations for energy harvesting system: (a) maximum steady-state voltage output in the frequency domain for the electromagnetic system; (b) maximum steady-state voltage output in the frequency domain for PEH system; (c) electromagnetic oscillator time response; (d) PEH time response.

differential equation with a stiff solver in state–space configuration was used to calculate the response. The solver ode15s was used because the output results exhibited a degree of stiffness and where ode45 did not yield efficient computing time. Based on the work by Aramendia *et al.* [26], the calculations were performed similarly where a harmonic apparent force of water was used to excite the bluff body of the hybrid harvester. The oscillations on the structure would produce strain on the piezoelectric and oscillations on the spring; both of which would result in the conversion into output electricity. The initial displacement, velocity, and acceleration were at zero, and the only parameter affecting the change was the force of the water hitting the oscillator. The parameters used in running the calculations are highlighted in Table 1. For this model, the cylinder bluff body was used and will continue to be used as a reference shape in subsequent studies.

The time responses of frequencies up to 80 Hz were calculated and the maximum amplitude at each frequency was used. Figure 4 shows the maximum harvestable voltage from the coupled system at steady state by analyzing the last half of the time response to remove transient effects. Figure 4(a) displays the electromagnetic oscillator system while Figure 4(b) displays the harvested voltage through the PEH system. This approach has been able to show the response in the frequency domain to approximate the resonant frequency.

Based on the results of the MATLAB simulation, a distinct peak in Figure 4(b) is seen for the PEH system in the frequency domain, which correlates to the natural frequency of the

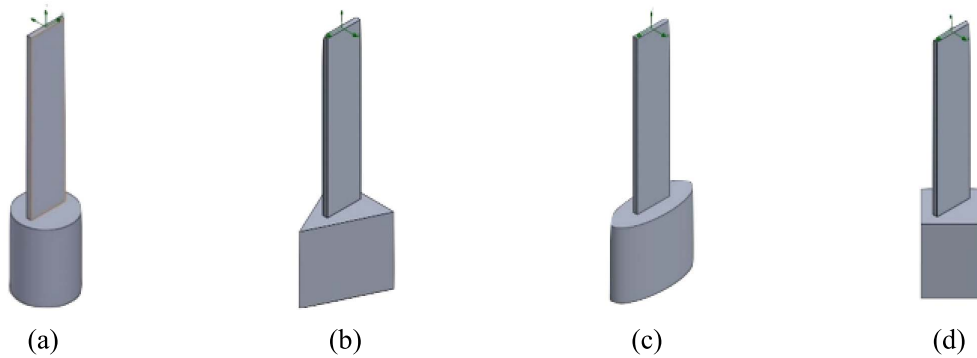


**Figure 5.** Different oscillator shapes tested in optimization: (a) cylinder; (b) triangular (normal); (c) ellipse; (d) quadrilateral.

structure that it is attached to. In contrast, Figure 4(a) shows two peaks that are measurable in the electromagnetic coupled system; the first peak corresponds to the resonant point of the electromagnetic oscillator and the second for the coupled PEH system. The natural frequency for the electromagnetic oscillator is 14 Hz whilst the PEH is 23 Hz; their time response is shown in Figures 4(c) and 4(d), respectively. By tuning the hybrid energy harvest into having the two resonant points closer to each other, the system can operate near to the natural frequency of both systems. Working near the structural resonance of the system is advantageous in maximizing the total power harvested from the surrounding flow of water. If both systems were tuned to resonate near the oscillation frequency because of FIV, then the hybrid energy harvester can continue to harvest maximum amounts of voltage through large displacements. Tuning is an additional parameter which can be introduced to increase the efficiency of the energy harvesting process for a coupled system shown in Figure 1(a).

## 5. Optimization studies

The four main proposed bluff-body shapes were the cylinder, triangle, ellipse, and quadrilateral. The added tip mass was modeled with a solid body and a beam as shown in Figure 5.

The bluff body serves a vital role in wake generation and creating turbulence behind the structure that increases power output from the hybrid harvester. Figure 6 shows the observed displaced amplitude modeled for the hybrid energy harvester when subjected to incoming external flow at 1.24 m/s. Vortices created behind a body are responsible for the vibration on the system of where vortex shedding leads to transverse oscillations on the structure relative to the water flow. The cylinder was first tested at a speed of 1.24 m/s and lower speeds as well to observe the formation of vortices behind the bluff body shown in Figure 6(a). The resultant displacement of the beam is perpendicular to the water flow since the directional stiffness is less in this direction than the direction parallel to the water flow, as shown in Figure 6(b).

Since the shape selection affects the formation and intensity of the turbulence disrupting the flow behind the bluff body, a CFD study was performed to illustrate the formation of these vortices. Figure 5 shows the motion of the vorticity generated behind the bluff body with similar surface areas of  $1600 \pm 1 \text{ mm}^2$ .

The addition of sharp edges generated more visible vorticity behind the shape; with the vorticity behind the triangle bluff body generating the most visible turbulence. In contrast, the smooth and thin shape of the ellipse does not generate as much turbulence. The maximum steady-state

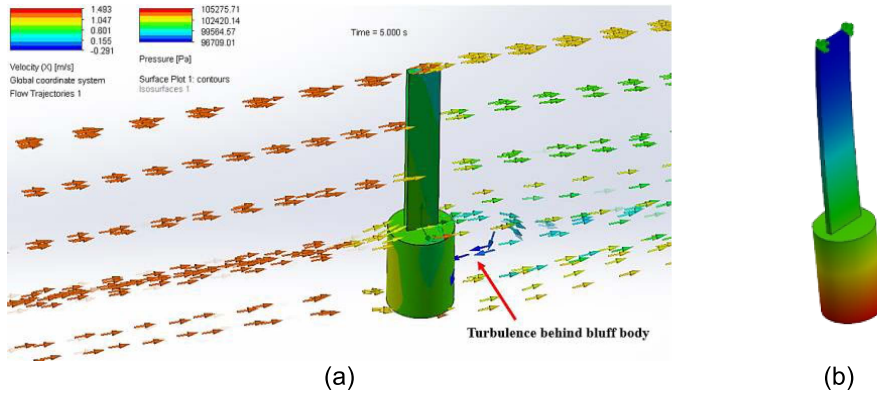


**Figure 6.** Isometric view of the simulation study on the cylinder oscillator configuration for energy harvesting: (a) fluid simulation at 1.24 m/s; (b) frequency study showing first mode shape.

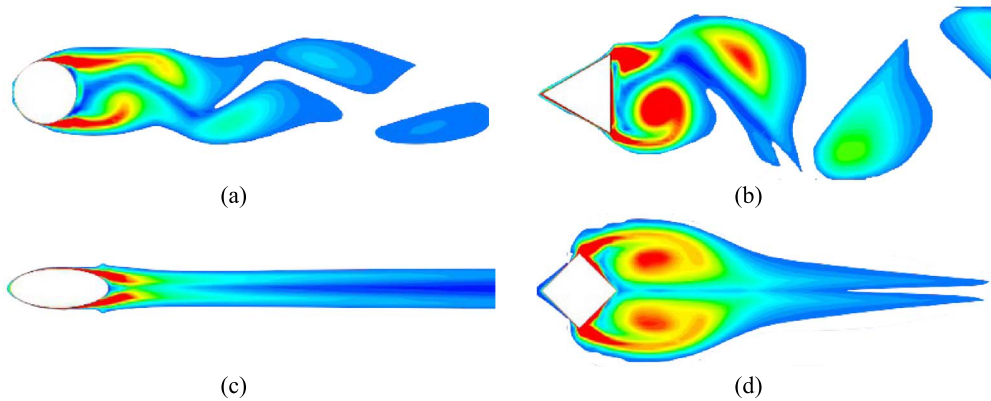


**Figure 7.** Measurable vorticity generated by bluff body: (a) circle; (b) triangle; (c) ellipse; (d) quadrilateral.

turbulence kinetic energy of the four shapes is summarized by Figure 8 below. While the triangular and quadrilateral bluff bodies have shown to generate significant amount of turbulence, the higher selected speeds could have introduced the effects of galloping past a certain onset water velocity which has been demonstrated in literature to aid in energy harvesting.

To investigate the effects of the turbulence formation only and avoid potential effects of pipe wall interaction harvester, the parameters of the study used is for external flow over the energy harvester bodies. This parameter study focussed on shape performance and did not have any attached piezoelectric materials or oscillator cavity. All iterations of the study were done with the shapes in Figure 3 having approximately the same mass of  $304.87 \pm 0.02$  g to ensure that the dynamic study and frequency study is also not affected by the differences in mass. The nonlinear dynamic study used the pressure effects of the fluid interaction with the structure and displays the flow effect on the structural quantities of stress, strain, and deformation during an 1 s period. Also, the frequency study looks at different mode shapes and corresponding resonant frequencies of each configuration. The resultant vibration in each first mode and the corresponding maximum, average, resultant amplitude can be compared. The simulated resonant frequency for the cylinder bluff body and modeled with the water flow is 25 Hz, which

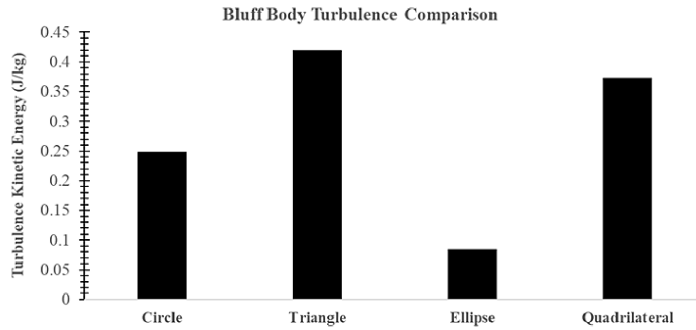


**Figure 8.** Maximum steady-state turbulence kinetic energy created behind bluff-body comparison.

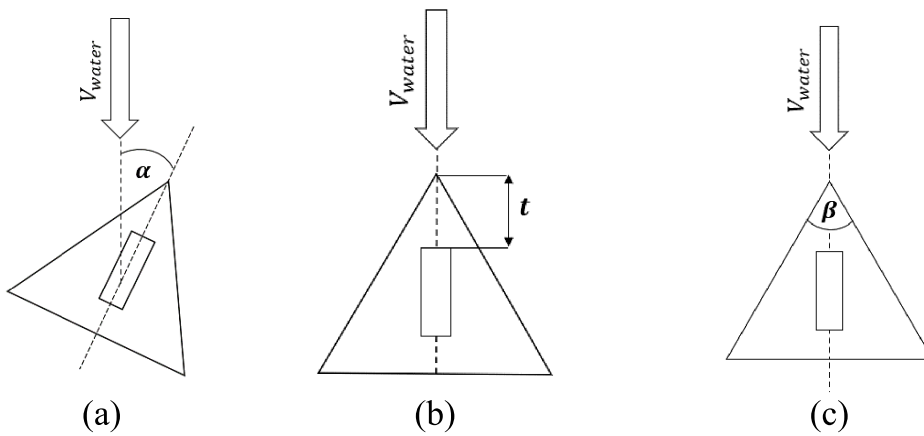


**Figure 9.** Parameters of change for optimization study: (a) rotation about axis; (b) distance of beam on oscillator; (c) internal angle variation.

**Table 5.** Parameters changed during optimization study

Parameters varied	Bluff-body shape	Range of variation	Reference figure
Rotation about the central axis	Triangle	0° to 90°	Figure 5(a)
	Ellipse	0°, 45° and 90°	
	Quadrilateral	0° (square) and 45°	
Beam placement from edge of body	Triangle	5 mm to 23 mm	Figure 5(b)
Internal angle relative to fluid flow	Triangle	16° to 75°	Figure 5(c)
Size ratio (length/width)	Ellipse	1 to 4	Figure 7

represents an 8.70% deviation from the derived MATLAB numerical solution. The cylindrical oscillator was selected as a control comparison since it does not have any changes in its geometry. The different parameters that were varied and the bluff-body shape studied are summarized in Table 5.

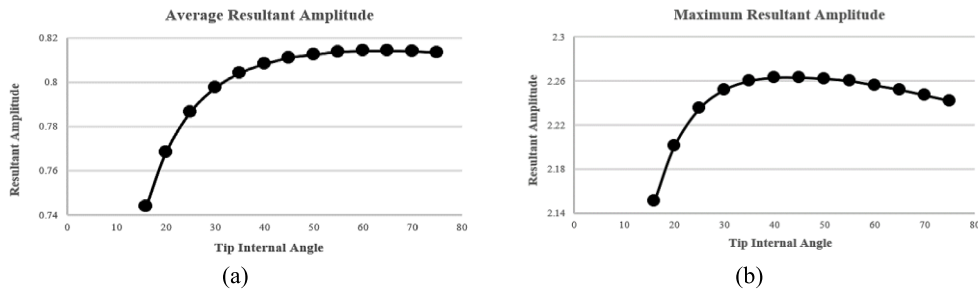


**Figure 10.** Optimization study results for a triangle-shaped oscillator for resonance performance in frequency study: (a) measured resultant average amplitude; (b) measured maximum resultant amplitude.

### 5.1. Optimization of the triangular bluff body

The triangular shape was first made using an equilateral triangle with its position placed in the middle of the axis of the beam. The study in optimizing the geometry of the triangle mainly differed in the angle of rotation from the axis (Figure 9(a)), placement of the beam on the triangle (Figure 9(b)), and angle of triangle tip (Figure 9(c)). For the study in the angle of attack through rotation of the beam along the axis Figure 9(a), the effect of the potential pressure difference between either side of the beam normal to the water flow was studied. During the frequency study comparison at the natural frequency of the harvester, there was no discernable change between the average and maximum resultant amplitude when changing the rotation angle. Moreover, beam placement on the equilateral triangular oscillator was studied; the distance in Figure 9(b) was varied between 5 mm to 23 mm and were constrained so that the beam was not placed outside the boundaries of the oscillator. However, the results of the frequency study indicated that at resonance, the placement of the beam did not affect the average and maximum resultant amplitude by a difference higher than 1.2%. As a result, both parameter changes are shown in Figures 7(a) and (b) did not have any further analysis. The final configuration applied to the triangle oscillator varied the internal angle at the tip where the edge impacting fluid is varied from 16° to 75°. This configuration change had the highest impact on the difference in average and maximum resultant amplitude with 4.95% and 8.62%, respectively. The conclusion from this optimization study was that the tip ranges between 40° to 65° were the most optimal internal angle for isosceles triangle oscillators in the parameter change shown in Figure 8. Further optimization studies into the triangular bluff body will require electromechanical coupling parameters by including a resistor across the piezoelectric energy harvester.

### 5.2. Optimization of ellipse bluff body

The study of the ellipse looked at the effect the difference in the length and width sizing parameters (Figure 11) had on the performance of the oscillator attached to the energy harvester. The frequency study demonstrated a small difference in varying ellipse sizing with the 1× ratio (circle) performing the worst and 2.5× performing the best at a difference of approximately 0.5% in the resultant amplitude. Moreover, the stress and strain plots as shown on Figures 12(a) and (b) point toward 2.5× having a significant amount of strain—which correlates to more voltage output through the piezoelectric patch. Also, the 2.5× ellipse sizing provided the highest strain on the beam after only 1 s in the dynamic simulation.

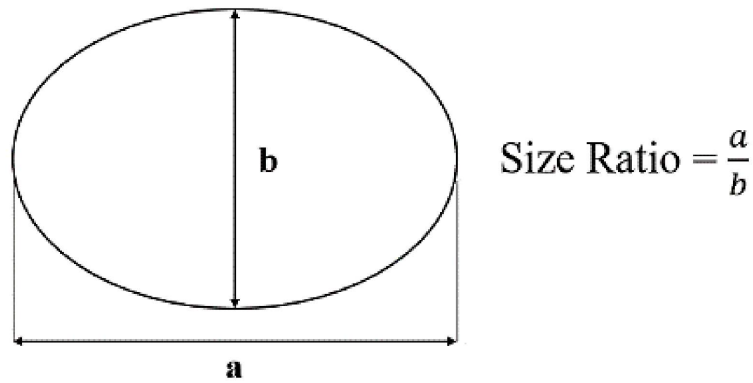


**Figure 11.** Ellipse size ratio optimization study parameter definition ( $a/b$  size ratio).

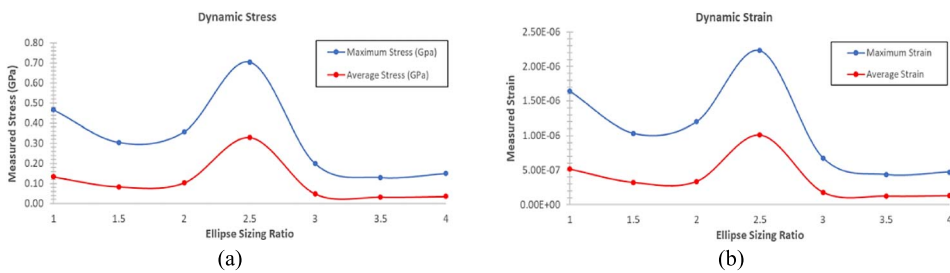


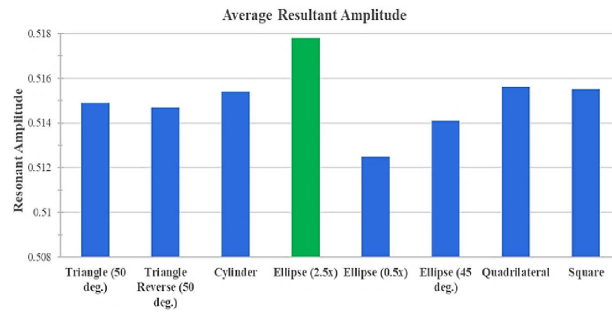
**Figure 12.** Nonlinear study for ellipse size ratio optimization: (a) dynamic stress; (b) dynamic strain.

### 5.3. Optimization of shape selection

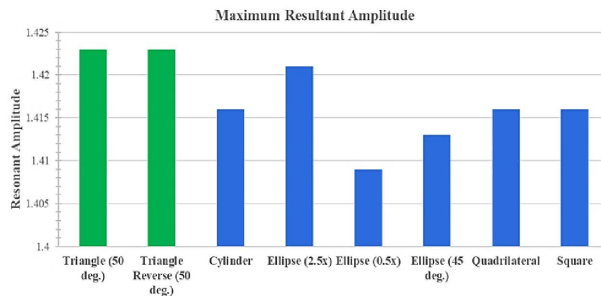
While the main objective of this study is to investigate different factors that can improve the hybrid energy harvester, it is also important to compare that to potential stresses that are exerted on the structure to visualize potential areas of failure or fatigue, while strain can be used to correlate piezoelectric performance. The figures presented in Figure 13 are based on the bluff-body configurations attached in Figure 5. “Triangle reverse” refers to a reverse flow direction, ellipse sizes were varied in size and angle of attack by 45° and “square” uses a bluff body in the shape of a square.

Figures 13(a) and (b) looked at the normalized frequency response of different bluff bodies with identical masses and measured the resultant amplitude at the beam. The results show average nodal values as well as the maximum nodal value along the beam which correlates to the energy harvesting piezoelectric patch would be attached to. The maximum resultant amplitude produced by the shape of the ellipse with the 2.5 size ratio for the average and maximum was visibly higher than the other shapes. While the ellipse did not generate a significant amount of turbulence based on the CFD study in comparison to the triangle or the cylindrical bluff body, this highlights that the mechanical structure also plays an important role in the energy harvesting performance under resonance.

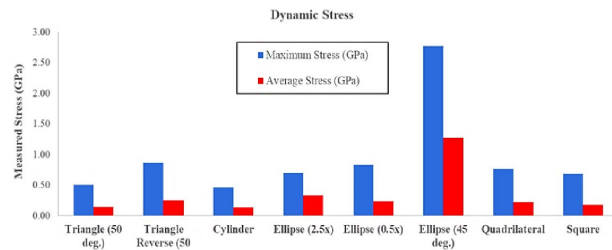
Figures 13(c) and (d) shows the finite element nonlinear dynamic structural study on the structure and measures the stress and strain on the beam after 1 s of simulated flow. The ellipse that was rotated at an orientation of 45° on the axis has the highest measurable stress, this is likely



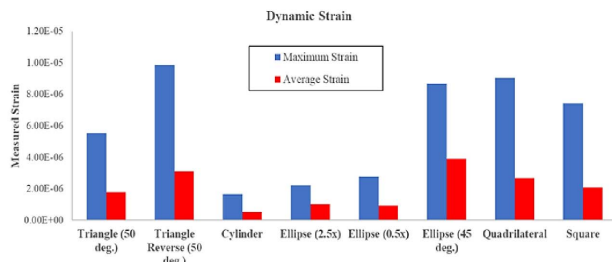
(a)



(b)



(c)



(d)

**Figure 13.** Shape performance optimization study from frequency study and dynamic study: (a) average resultant amplitudes; (b) maximum resultant amplitudes; (c) dynamic stress; (d) dynamic strain.

due to the structure that channels the water flow more along one side and generates a higher pressure difference across both sides which leads to a higher dynamic deflection and forces the formation of vortices and turbulence behind the bluff body. Although the vortex shedding phenomenon for a cylinder bluff body is a well-researched topic, the effects of wake galloping after the onset minimum velocity has shown how triangular bluff bodies can also harvest more energy. Also, the placement of the beam on the bluff body highlights the opportunities for more optimization that enables the elliptical bluff body producing small turbulence to have the highest average resultant amplitude under resonance.

Overall, the simulation study showed that the oscillator with a triangle and ellipse shape outperforms the cylinder orientation at 1.24 m/s velocity when comparing values that correlates to the potential energy harvested by a piezoelectric beam that the initial model was developed on. Both the fluid and structural interaction because of vortex shedding also plays a major role in the oscillator's performance to generate the vibration required to excite the energy harvester. Consequently, the triangle-shaped bluff body has an abrupt change in which the flow of water generates vortices because of the discontinuity in the wake of the edges of the shape. The overall pressure difference around the shape leads to FIV on the structure.

## 6. Conclusion

In the present study, a new compact design of a hybrid energy harvester that uses a piezoelectric and electromagnetic system was developed for use in submerged pipe flow applications. The addition of a tip mass provides a housing for the electromagnetic oscillator but also generates turbulence that is used to generate power. First, a mathematical model was developed for the coupled systems that also includes an electromechanical coupling when the harvester was subjected to transverse oscillations because of FIV. Afterward, a numerical solver was able to get the time and frequency response of the hybrid harvester. From these results it was shown that tuning the systems to resonate close to each other, the voltage harvested can be increased. If the resonant point of both systems is tuned to the oscillation frequency of the water flow, then the energy harvested will also be maximized. Then, a computational simulation was performed to observe the vortex shedding behind a cylindrical body by using an unsteady  $k-\omega$  SST model over 20 s. After validating the convergence of CFD results, the simulation was then expanded for triangular, elliptical, and quadrilateral bluff-body shapes. At 1.24 m/s the first mode shape of the energy harvester oscillates perpendicular to the water flow because of the beam orientation having different area moment of inertias. An optimization study was done across different bluff-body shapes and the performance of the bluff body alone as well as the harvester structure was compared. The tip triangle angle presented the highest amplitude oscillations when  $40^\circ < \beta < 65^\circ$ . The isosceles size ratio was also compared and found that  $2.5\times$  ratio experienced the greatest strain along the beam where the piezoelectric material is to be attached to. While the ellipse generated the least turbulence, the performance of the  $2.5\times$  ratio ellipse (average resultant amplitude) and isosceles triangles (maximum resultant amplitude) performed the best during resonance with the frequency study. This suggests the importance of the fluid-structure interaction on the beam as well as the galloping and VIV effects for noncylindrical bodies.

## Acknowledgment

This work is supported by International Research Collaboration Co-Funds (IRCC-2020-017) from Qatar University.



## References

- [1] H. A. Sodano, D. J. Inman, G. Park, "Generation and storage of electricity from power harvesting devices", *J. Intell. Mater. Syst. Struct.* **16** (2005), no. 1, p. 67-75.
- [2] A. Muthalif, D. Nordin, "Optimal piezoelectric beam shape for single and broadband vibration energy harvesting: modeling, simulation and experimental results", *Mech. Syst. Signal Process.* **54-55** (2015), p. 417-426.
- [3] D. T.-F. Betono, I. Aramendia, J. Martinez-Rico, U. Fernandez-Gamiz, E. Zulueta, "Piezoelectric energy harvesting controlled with an IGBT H-Bridge and Bi-directional Buck-Boost for Low-Cost 4G Devices", *Sensors* **20** (2020), no. 24, article no. 7039.
- [4] D. K. Bhardwaj, D. K. Tyagi, "Effect of tip masses and its position on the power by piezoelectric material", *Int. J. Eng. Sci. Comput.* **9** (2019), no. 4, p. 21336-21342.
- [5] R. Song, X. Shan, F. Lv, T. Xie, "A study of vortex-induced energy harvesting from water using PZT piezoelectric cantilever with cylindrical extension", *Ceram. Int.* **41** (2015), no. 1, p. S768-S773.
- [6] M. Safaei, H. Sodano, S. Anton, "A review of energy harvesting using piezoelectric materials: state-of-the-art a decade later (2008-2018)", *Smart Mater. Struct.* **28** (2019), no. 11, article no. 113001.
- [7] A. Khalak, C. H. K. Williamson, "Motions, forces and mode transitions in vortex-induced vibrations at low mass-damping", *J. Fluids Struct.* **13** (1999), p. 813-851.
- [8] C. H. K. Williamson, R. Govardhan, "Vortex-induced vibrations", *Annu. Rev. Fluid Mech.* **36** (2004), p. 413-455.
- [9] T. Sarpkaya, "A critical review of the intrinsic nature of vortex-induced vibrations", **19** (2004), p. 389-447.
- [10] P. W. Bearman, "Circular cylinder wakes and vortex-induced vibrations", *J. Fluids Struct.* **27** (2011), p. 648-658.
- [11] X. Gao, W. Shih, W.-H. Shih, "Flow energy harvesting using piezoelectric cantilevers with cylindrical extension", *IEEE Trans. Indust. Electron.* **60** (2013), p. 1116-1118.
- [12] S. Pobering, S. Ebermeyer, N. Schwesinger, "Generation of electrical energy using short piezoelectric cantilevers in flowing media", *Act. Pass. Smart Struct. Integ. Syst.* **7288** (2009), p. 109-116.
- [13] J. Jia, X. Shan, D. Upadrashta, T. Xie, Y. Yang, R. Song, "Modeling and analysis of upright piezoelectric energy harvester under aerodynamic vortex-induced vibration", *Micromachines* **9** (2018), no. 12, article no. 667.
- [14] J. Wang, L. Geng, L. Ding, H. Zhu, D. Yurchenko, "The state-of-the-art review on energy harvesting from flow-induced vibrations", *Appl. Energy* **267** (2020), article no. 114902.
- [15] I. Aramendia, A. Saenz-Aguirre, A. Boyano, U. Fernandez-Gamiz, E. Zulueta, "Oscillating U-shaped body for underwater piezoelectric energy harvester power optimization", *Micromachines* **10** (2019), article no. 737.
- [16] A. Abdelkefi, Z. Yan, M. R. Hajj, "Performance analysis of galloping-based piezoaeroelastic energy harvesters with different cross-section geometries", *J. Intell. Mater. Syst. Struct.* **25** (2014), no. 2, p. 246-256.
- [17] H. D. Akaydin, N. Elvin, Y. Andreopoulos, "The performance of a self-excited fluidic energy harvester", *Smart Mater. Struct.* **21** (2012), no. 2, article no. 025007.
- [18] W. Sun, D. Zhao, T. Tan, Z. Yan, P. Guo, X. Luo, "Low velocity water flow energy harvesting using vortex induced vibration and galloping", *Appl. Energy* **251** (2019), article no. 113392.
- [19] W. Sun, T. Tan, Z. Yan, D. Zhao, X. Luo, W. Huang, "Energy harvesting from water flow in open channel with macro fiber composite", *AIP Adv.* **8** (2018), article no. 095107.
- [20] V. Challa, M. Prasad, E. T. Fisher, "A coupled piezoelectric-electromagnetic energy harvesting technique for achieving increased power output through damping matching", *Smart Mater. Struct.* **178** (2009), no. 9, article no. 095029.
- [21] H. Mirab, R. Fathi, V. Jahangiri, M. M. Etefagh, R. Hassannejad, "Energy harvesting from sea waves with consideration of airy and JONSWAP theory and optimization of energy harvester parameters", *J. Mar. Sci. Appl.* **14** (2015), no. 4, p. 440-449.
- [22] J. Zhao, H. Zhang, F. Su, Z. Yin, "A novel model of piezoelectric-electromagnetic hybrid energy harvester based on vortex-induced vibration", in *2017 International Conference on Green Energy and Applications (ICGEA), Singapore (IEEE)*, 2017, p. 105-108.
- [23] L. B. Zang, A. Abdelkefi, H. L. Dai, R. Naseer, L. Wang, "Design and experimental analysis of broadband energy harvesting from vortex-induced vibrations", *J. Sound Vib.* **408** (2017), p. 210-219.
- [24] D. Tripathi, *Practical Guide to Polypropylene*, Rapra Technology Ltd., Shawbury, Shrewsbury, Shropshire, 2002.
- [25] C. Maier, T. Calafut, *Polypropylene: The Definitive User's Guide and Databook*, William Andrew Publishing House, Norwich, New York, USA, 1999.
- [26] I. Aramendia, U. Fernandez-Gamiz, E. Zulueta Guerrero, J. M. Lopez-Guede, J. Sancho, "Power control optimization of an underwater piezoelectric energy harvester", *J. Appl. Sci.* **8** (2018), no. 3, article no. 389.
- [27] I. S. Dauda, A. Muthalif, N. Diyana, T. Saleh, "Comparative study of conventional and magnetically coupled piezoelectric energy harvester to optimize output voltage and bandwidth", *J. Microsyst. Technol.* **23** (2016), no. 7, p. 2663-2674.
- [28] A. K. Soti, M. C. Thompson, J. Sheridan, R. Bhardwaj, "Harnessing electrical power from vortex-induced vibration of a circular cylinder", *J. Fluids Struct.* **70** (2017), p. 360-373.

- [29] G. Donoso, C. L. Ladera, P. Martin, "Magnetically coupled magnet-spring oscillators", *Eur. J. Phys.* **31** (2010), no. 3, p. 433-452.
- [30] ANSYS, *Ansys Academic Fluent, Release 2020 R2*, Canonsburg, Pennsylvania, 2020.
- [31] F. R. Menter, "Two-equation eddy-viscosity turbulence models for engineering applications", *Amer. Inst. Aeronaut. Astronaut.* **32** (1994), no. 8, p. 1598-1605.
- [32] P. J. Roache, "Quantification of uncertainty in computational fluid dynamics", *Annu. Rev. Fluid Mech.* **29** (1997), p. 123-160.
- [33] A. Roshko, "Experiments on the flow past a circular cylinder at very high Reynolds number", *Fluid Mech.* **10** (1961), no. 3, p. 345-356.
- [34] C. Norberg, "Fluctuating lift on a circular cylinder: review and new measurements", *Fluids Struct.* **17** (2003), no. 1, p. 57-96.